J Neurosurg 103:891–902, 2005

Flow changes caused by the sequential placement of stents across the neck of sidewall cerebral aneurysms

GÁDOR CANTÓN, PH.D., DAVID I. LEVY, M.D., JUAN C. LASHERAS, PH.D., AND PETER K. NELSON, M.D.

Department of Mechanical and Aerospace Engineering, University of California; Department of Neurosurgery, Kaiser Permanente Medical Center, San Diego, California; and Departments of Radiology and Neurosurgery, New York University School of Medicine, New York, New York

Object. The goal of this study was to quantify the reduction in velocity, vorticity, and shear stresses resulting from the sequential placement of stents across the neck of sidewall cerebral aneurysms.

Methods. A digital particle image velocimetry (DPIV) system was used to measure the pulsatile velocity field within a flexible silicone sidewall intracranial aneurysm model and at the aneurysm neck–parent artery interface in this model. The DPIV system is capable of providing an instantaneous, quantitative two-dimensional measurement of the velocity vector field of "blood" flow inside the aneurysm pouch and the parent vessel, and its changes at varying stages of the cardiac cycle. The corresponding vorticity and shear stress fields are then computed from the velocity field data. Three Neuroform stents (Boston Scientific/Target), each with a strut thickness between 60 and 65 μm, were subsequently placed across the neck of the aneurysm model and measurements were obtained after each stent had been placed.

The authors measured a consistent decrease in the values of the maximal averaged velocity, vorticity, and shear stress after placing one, two, and three stents. Measurements of the circulation inside the sac demonstrated a systematic reduction in the strength of the vortex due to the stent placement. The decrease in the magnitude of the aforementioned quantities after the first stent was placed was remarkable. Placement of two or three stents led to a less significant reduction than placement of the first stent.

Conclusions. The use of multiple flexible intravascular stents effectively reduces the strength of the vortex forming in an aneurysm sac and results in a decrease in the magnitude of stresses acting on the aneurysm wall.

KEY WORDS • hemodynamics • intracranial aneurysm • sidewall aneurysm • stent • wall stress

PLACEMENT of intravascular stents across the aneurysm neck is currently used in conjunction with packing the lumen of the lesion with coils in the case of complex wide-necked aneurysms. The stent acts as a rigid endoluminal scaffold that prevents coil herniation into the parent vessel. Lanzino, et al.,[11] have reported that stent placement in this setting also changes the intraaneurysm hemodynamics, preventing or reducing coil compaction.

Based on preliminary clinical experience and experimental studies, investigators have postulated that simply crossing an aneurysm with one or more stents may disturb blood flow within the aneurysm sac sufficiently to promote a reduction in the intraaneurysm flow velocity and the formation of a stable thrombus, leading to uncoupling of the aneurysm from the parent vessel.[5,7,10,13,19,20]

Because there are very few case reports on successful aneurysm occlusion following the use of only one stent, it has been suggested that aneurysm thrombosis may be accelerated by using multiple stents, which would reduce the porosity associated with a single one. In fact, there are some reported cases[3,5] in which reduction of the inflow due to the placement of two stents was sufficient to accelerate the healing process.

In this study our aim was to investigate changes in the velocity field inside the aneurysm sac as well as the hemodynamic forces within the aneurysm resulting from the implantation of one, two, and three stents without the use of coils or other packing agents. For this purpose, a DPIV technique was used to measure the pulsatile blood velocity field at the entrance and inside the sac of a silicone model of a sidewall aneurysm with a prototypical shape. Measurements were first obtained in the untreated model (control) and again after placing each of the three stents (experimental models). Shear stresses were computed in each case.

Materials and Methods

A 10-mm sidewall aneurysm arising from a 4-mm vessel was created.[9] The geometric dimensions of the sidewall aneurysm and the parent vessel harboring the aneurysm are shown in Fig. 1.

Three flexible Neuroform stents (Boston Scientific/Target, Fremont, CA), which had been subjected to a brief surface oxidation to diminish light reflectivity, were placed across the aneurysm neck; measurements were taken after the implantation of each stent. Each

Abbreviations used in this paper: DPIV = digital particle image velocimetry; 2D = two-dimensional; 3D = three-dimensional.

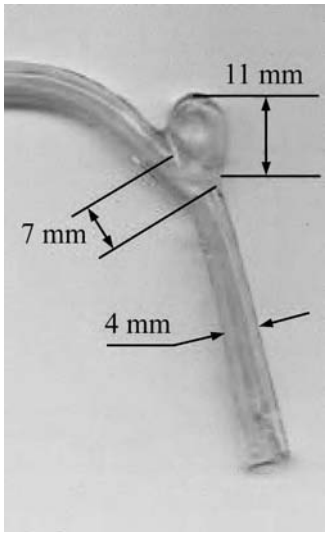

FIG. 1. Photograph showing the sidewall aneurysm model and geometrical data relevant to the study.

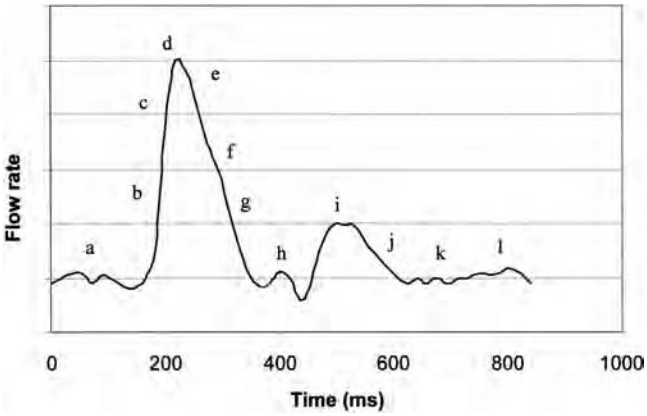

FIG. 2. Graph showing the waveform corresponding to flow in the carotid artery, which was supplied to the sidewall aneurysm model.

successive stent was placed such that the aneurysm neck was fully covered by the device. All stents engaged the parent vessel approximately 6 to 7 mm proximal and distal to the aneurysm. There was no attempt to align the stent struts in any specific orientation.

The experimental setup has been described elsewhere[4] and is only summarized here. The aneurysm model was perfused with a mixture of deionized water and ethylene glycol (with a density of 1.045 g/ml and a viscosity of 2.5 centipoises at room temperature), which had been seeded with lycopodium powder (Carolina Biological Supply Company, Burlington, NC) having a mean diameter ranging between 1 and 10 μm. To avoid distortion of the visualized flow by refraction, the model was placed in a transparent box filled with the same perfusion fluid.

A pulsatile flow corresponding to the flow through the carotid artery (Fig. 2) was supplied to the model by means of a pulsatile pump (UHDC flow system; Sidac Engineering, London, ON, Canada). The peak volume rate selected for this study was 360 ml/minute. The duration of the pulsatile flow was 0.83 second, corresponding to a cardiac rate of 72 beats per minute.

A DPIV system (TSI Inc., St. Paul, MN) was used to quantify the instantaneous 2D velocity field inside the aneurysm model. For each cardiac cycle, 12 or 13 pairs of images were obtained at the times indicated in Fig. 2 (a–l on the flow waveform; measuring rate 15 pairs of images/second). The velocity field was then computed with the aid of appropriate software (Insight; TSI Inc.) by cross-correlating the two images and measuring the particle displacements from statistical correlations of each pair of images. Once the velocity field had been computed, the data were processed by appropriate software (Tecplot; Amtec Engineering, Inc., Bellevue, WA) to compute other flow quantities such as the vorticity, strain rate fields, and circulation.

Results

The changes in the intraaneurysm hemodynamics due to the subsequent placement of three stents across the neck of a sidewall aneurysm are reported in this section.

To identify these hemodynamic changes, measurements of the velocity, vorticity, and rate of strain in the aneurysm sac obtained after placement of each stent were compared with corresponding measurements obtained in the control model. Although the flow in an aneurysm sac is 3D and not confined to any particular plane, we measured the velocity field in an axial plane running along the midline of the aneurysm and dissecting the aneurysm sac at a midpoint to conduct a significant comparison. The measured cross-plane is shown in Fig. 1.

Control Model

Velocity Field. Figure 3 shows measurements of the 2D velocity field in the parent vessel and inside the aneurysm sac corresponding to one cardiac cycle. The *green arrows* indicate both the magnitude and direction of the measured velocities. These measurements were obtained 1/15 second apart from each other at specified points along the cardiac cycle shown in Fig. 2.

We observed that due to the curvature of the parent vessel, the stream diverged away from the wall before it entered the aneurysm. The stream then impinged on the distal neck of the aneurysm, splitting into two streams: a jet entering the aneurysm along the distal wall and a stream flowing through the parent vessel (Fig. 4).

At the end of the acceleration phase (that is, the peak systole [Fig. 5d]), a strong 3D vortex formed inside the aneurysm sac, inducing a clockwise rotational motion inside the sac. The core of the vortex was initially located near the distal neck of the aneurysm, but later it progressively moved along the distal wall toward the fundus. At the end of the diastole (Fig. 5j–l), this vortex had mostly dissipated, although a residual rotational motion could still be observed.

The flow rate of the fluid present in the aneurysm drastically decreased from maximal values during the peak systole to lower values at the late stage of the systole and at the peak diastole. This outflow merged with the main flow in the parent vessel, forming a helical vortex downstream of the aneurysm, as shown in Fig. 4.

In this model of a sidewall aneurysm, the measured velocity of the jet entering the aneurysm at this plane was considerably lower than that measured in the parent vessel during most of the cardiac cycle. In fact, at any given instant of time in the cardiac cycle, the magnitude of velocity at the entrance to the sac may reach the values measured at the proximal wall of the sac, which are 10% of the velocities in the parent vessel. Only during the deceleration phase of the systole (Fig. 5d–f) did the magnitude of the velocity seem

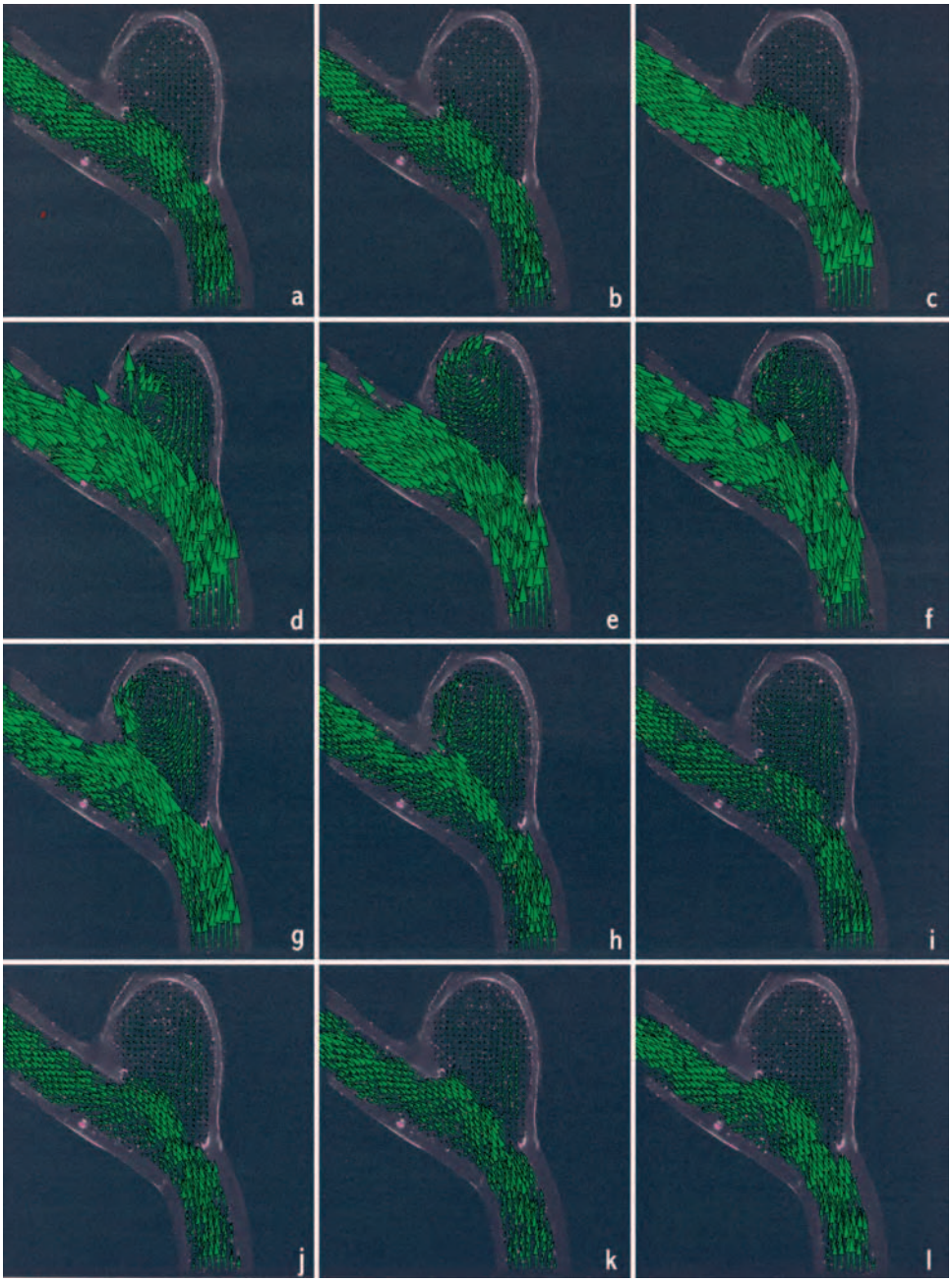

FIG. 3. Images obtained using the DPIV system showing the velocity field in the parent artery as well as within the aneurysm sac throughout the cardiac cycle. Panels correspond to the stages (a–l) indicated in Fig. 2.

to reach a maximal value of 60 to 70% of the velocity of flow in the parent vessel. This maximal velocity of the jet as it entered the sac at the peak systole was consistently (with no cycle-to-cycle change) located at the distal half of the sac, toward the distal wall and close to the fundus, and it was concentrated in a very small area.

Vorticity Field. The 2D component of the vorticity field ($w_z = 0.5[\partial u/\partial y - \partial v/\partial x]$) corresponding to measurements shown in Fig. 5 is given in Fig. 6. The isocontours of the vorticity vector are indicated by varying intensities of red (counterclockwise vorticity) and blue (clockwise vorticity). These measurements show that the vorticity differed greatly at the proximal and distal walls of the aneurysm. It reached maximal values—as well as maximal spatial gradients—at the peak systole along the distal wall. These values were associated with the presence of the strong vortex located near this wall of the aneurysm. At the end of the cycle, the vorticity in this distal region decreased to negligible values. At the proximal wall, the vorticity values were quite low throughout the cardiac cycle, but never negligible, except at the neck where there were significant temporal gradients (note the changes in the values at Points c and d of the cardiac cycle [Fig. 2]).

Shear Stress Field. We also measured the shear stresses

FIG. 4. Schematic drawing showing the effect of the flow pattern in the aneurysm sac downstream from the parent vessel.

inside the aneurysm sac (Fig. 7). The shear stress field exhibited several important features due to the eccentric location of the vortex core. First, it is important to note the significant difference between stresses acting on the proximal and distal walls of the aneurysm. The proximal wall of the aneurysm was subjected to relatively low shear stresses with no significant spatial or temporal gradients except at the neck, where we measured temporal gradients of shear stresses. At the distal wall, however, larger gradients of wall shear stresses were measured because of the presence of the vortex core. This wall region is characterized by large gradients and, most important, a reversed direction of the wall shear stresses (τ_w). The largest spatial gradients were observed at the peak systole and during the deceleration of the systole, which were the stages of the cardiac cycle at which the vortex displayed its maximal strength. The distal wall was also a region where the most significant temporal gradients of wall shear stresses were observed. These reached a maximal value at the peak systole (Fig. 7d) and then decayed to a negligible value at the end of the cycle (Fig. 7k or l). Finally, the fundus was subjected to extremely low values of shear stresses for most of the cardiac cycle, with small temporal and spatial gradients of these stresses.

In summary, we observed the formation of a very strong 3D vortex located at the distal half of the aneurysm sac. We identified regions of large wall shear stresses near the distal neck and along the distal wall of the aneurysm. Furthermore, we observed that the complex 3D vortex flow resulted in spatial and temporal gradients of these wall shear stresses.

Multiple Stent Models

We obtained a set of measurements that was identical to the one presented for the control model, after consecutive placement of three Neuroform stents. That is, we measured the flow field within the entire aneurysm sac, preserving the flow conditions and flow waveform input to the parent vessel. A comparative summary of the resulting velocity, vorticity, and stress fields is presented here. The measurements consisted of an ensemble averaged over four cardiac cycles to minimize any error due to cycle-to-cycle variability. To be able to determine precise hemodynamic changes due to the placement of multiple stents, we systematically identified the maximal values of velocity, vorticity, and stresses within the aneurysm sac, values that were always located at the distal aneurysm neck. We then compared those averaged values of the maximal velocity, vorticity, and stresses measured at the distal neck for the stented (experimental) model and the control model.

Velocity Field. There were certain hemodynamic features of the velocity field that persisted after we placed one, two, or even three stents (Fig. 8). First, the flow around the proximal wall and the fundus was nearly stagnant throughout the cardiac cycle, whereas the velocities at the distal region changed in accordance with the cardiac cycle, reaching maximal values (that decreased with the number of stents) at the peak systole and minimal values (even lower than the velocities measured at the proximal wall) at the end of the cycle. Second, at the peak systole, a relatively strong vortex was always seen forming at the distal neck of the aneurysm, and the clockwise rotational motion, which was observed in the control model, remained even after the third stent had been placed. Third, during the diastole, the vortex dissipated and a near stasis was achieved inside the sac at the end of the cycle.

We also observed several important differences in the velocity field while placing the stents (Fig. 8). As previously described for the control model, the core of the vortex was predominantly located near the distal wall. Placement of one stent did not change the vortex location; however, when two or three stents had been placed, the core of the vortex migrated slightly toward the center of the sac and became weaker. Specifically, the presence of the third stent led to a considerably perturbed rotational motion inside the aneurysm sac and to a more random nonrepetitive pattern from cycle to cycle.

To provide a quantification of the effect of placing each stent, we measured the values of the velocity field at the peak systole and at the end of the cycle and averaged them over four cardiac cycles. Table 1 shows a comparison of the maximal mean velocity magnitudes for the control model as well as for the experimental models after placement of one, two, and three stents. At the peak systole, we measured a 40% reduction in the maximal value of the velocity after the first stent had been placed, and a 60% reduction after the third stent had been placed. This reduction was more striking at the end of the diastole, with a 76% decrease demonstrated after the first stent had been placed and almost an 80% drop in the maximal velocity value after all three stents had been inserted.

Shear Stress Field. With respect to stress measured in the proximal wall, due to the eccentric location of the vortex core, stresses in the distal wall were consistently much greater, although they decreased in magnitude with the number of the stents that had been implanted. This difference caused gradients of wall shear stresses along the wall of the aneurysm sac to become higher at the peak systole

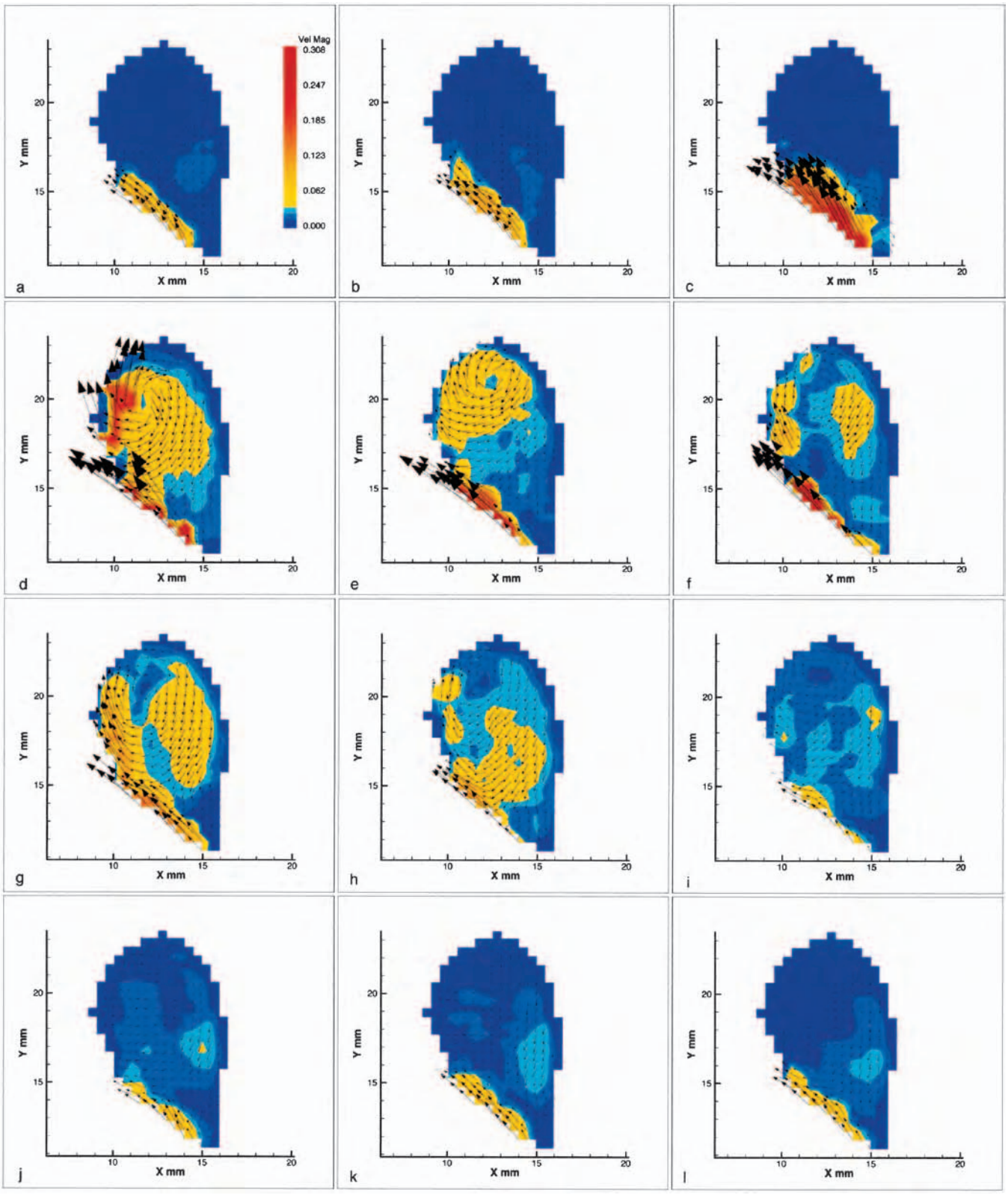

FIG. 5. Images generated by the DPIV system showing the velocity magnitude field (m/second) inside the aneurysm sac throughout the cardiac cycle. Panels correspond to the stages indicated in Fig. 2.

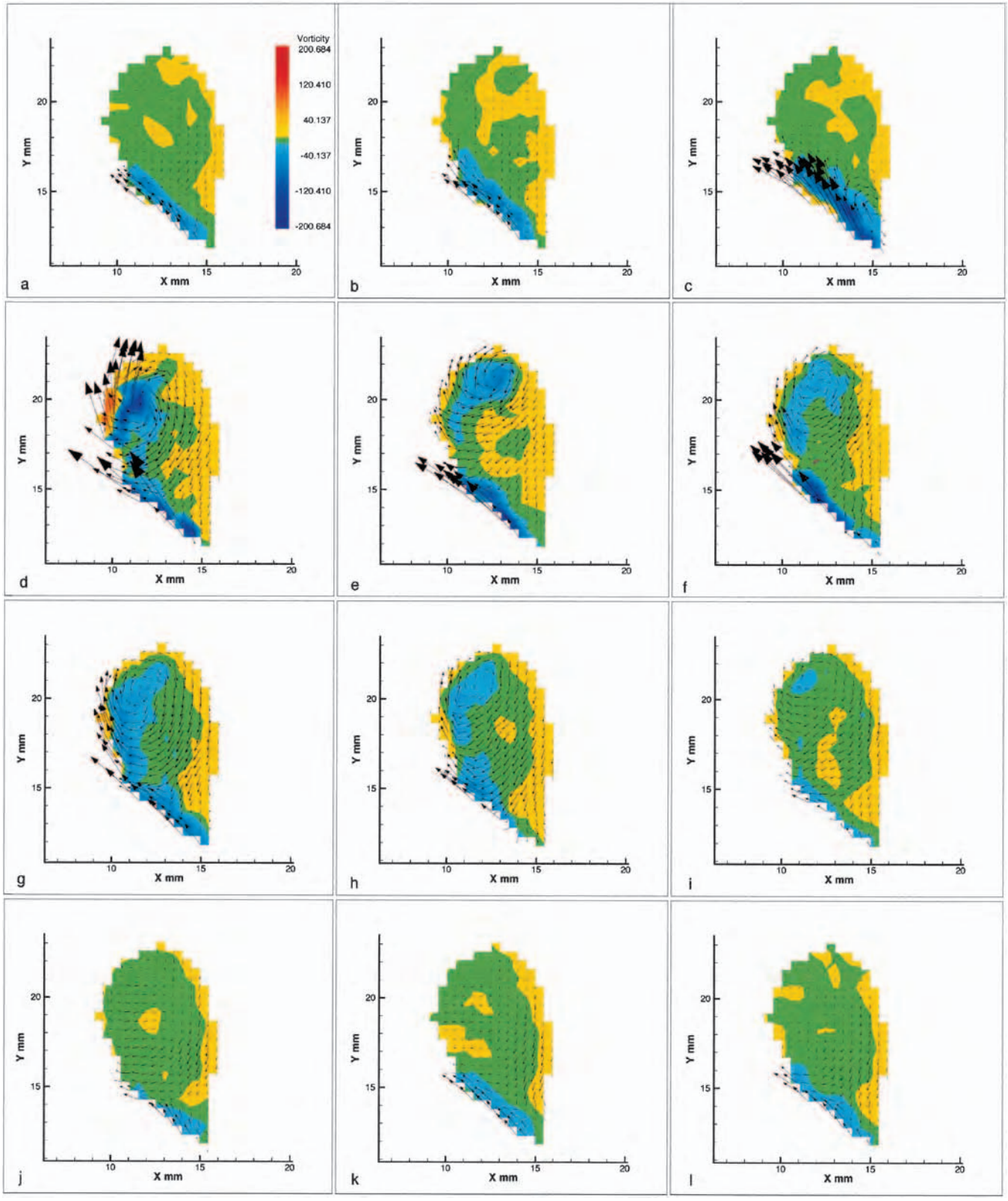

FIG. 6. Images generated by the DPIV system showing the vorticity field (1/second) inside the aneurysm sac throughout the cardiac cycle. Panels correspond to the stages indicated in Fig. 2.

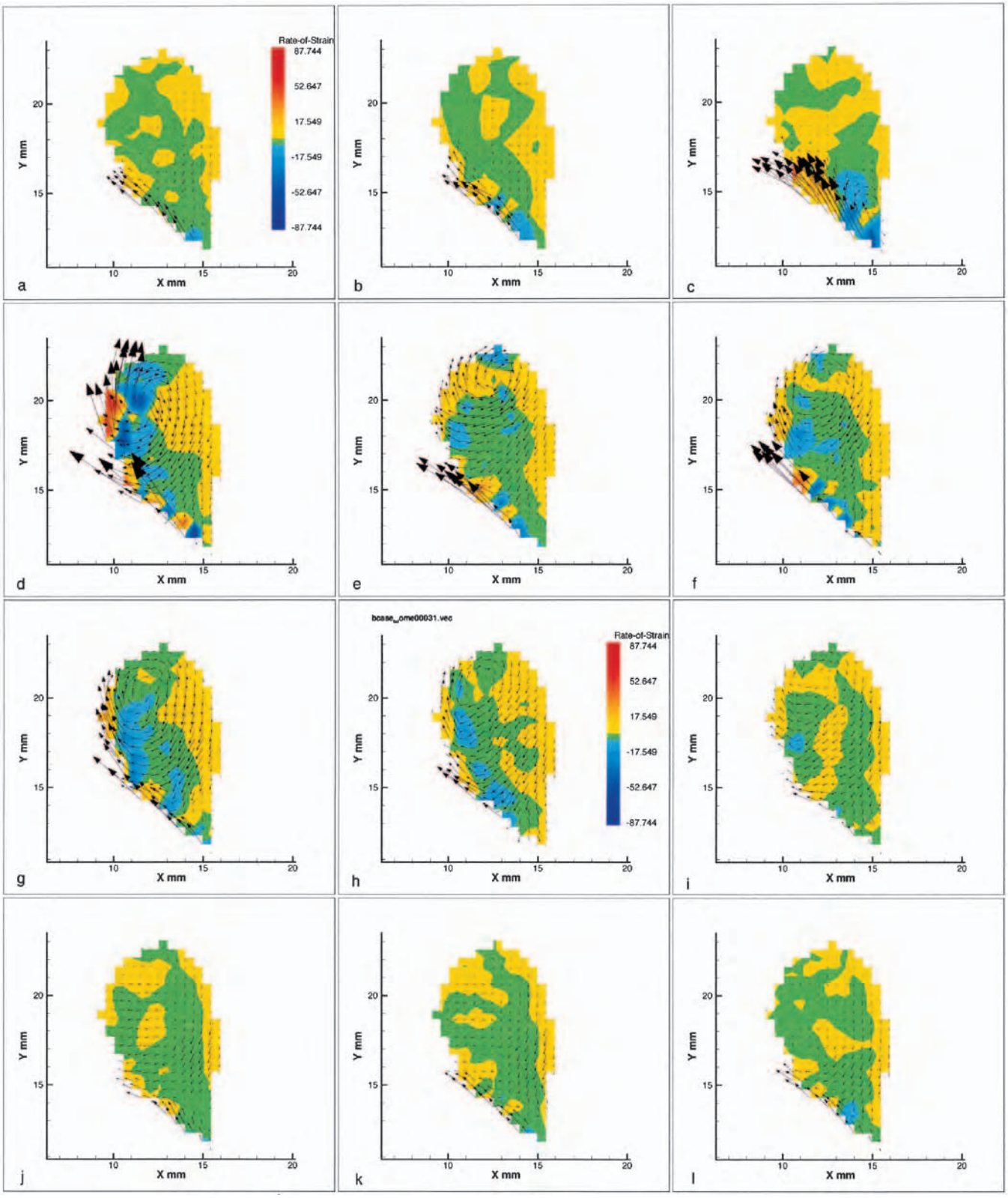

FIG. 7. Images generated by the DPIV system showing the stress field (1/second) inside the aneurysm sac of the control model. Panels correspond to the stages indicated in Fig. 2.

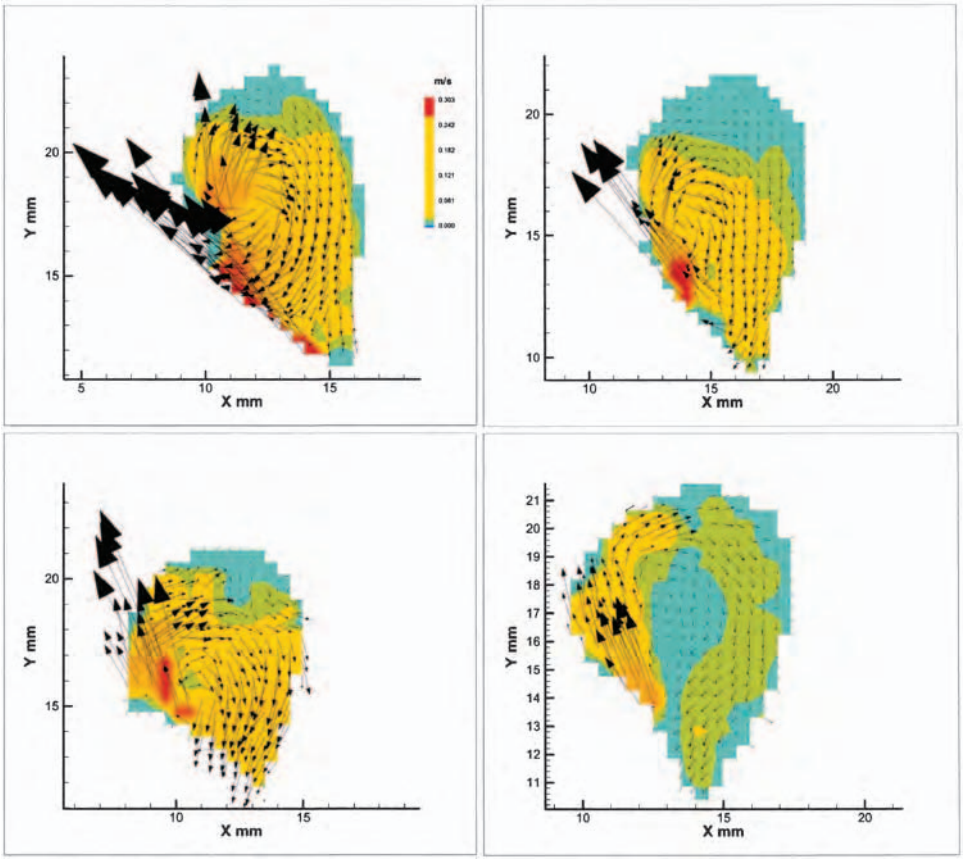

FIG. 8. Graphs showing a comparison of the velocity fields at the peak systole corresponding to the control model *(upper left)* and the experimental models after placement of one *(upper right)*, two *(lower left)*, and three *(lower right)* stents.

and during the deceleration portion of the systole, when shear stresses at the distal wall reached values up to 10 times greater than those measured at the proximal wall at those stages in the cycle. Nevertheless, after placement of the third stent these gradients are less significant. At the end of the cycle, the measured values of stresses at the distal wall were of the same order as the ones at the proximal wall, leading to extremely high temporal gradients of wall shear stresses at the distal wall of the aneurysm sac (Fig. 9).

We also measured, in all stented (experimental) models, gradients of wall shear stresses at the fundus of the sac that were similar to those encountered at the distal wall. The magnitude of these stresses, however, seemed to be significantly reduced after placement of the third stent.

A comparison of measured values of the maximal averaged stresses at the peak systole and the end of the cycle is summarized in Table 1. At the peak systole, there was a systematic decrease in maximal shear stresses with the number of stents, achieving a total reduction of 72% after placement of the third stent. This decrease was not that obvious at the end of the cycle, probably because of the low values that were measured, which were of the same order as the measurement error.

Vorticity Field. We also measured the vorticity field inside the sac after each stent was inserted. Figure 10 shows a comparative summary of our measurements. As was the case with the stress field, we observed that the location of the vortex core led to a considerable difference in the vorticity values at each of the aneurysm walls. At the peak systole, in all experimental models we measured values of vorticity that were larger at the distal wall than those measured at the proximal wall. After one stent had been placed, the values measured at the distal wall were 30 times greater than the values measured at the proximal wall. We also measured large spatial and temporal gradients at the distal wall and in the fundus, whereas at the proximal wall we measured very small values of vorticity throughout the cardiac cycle.

Table 1 shows that the effect of stent placement on the vorticity was more noticeable at the end of the cycle, when the vorticity was decreased by 80% after placing three stents. This decrease was less obvious at the peak systole.

Circulation. To quantify the effect of stents on flow inside the aneurysm sac further, we measured the strength of the vortex by computing the circulation (Γ). The circulation is defined as the following:

$\Gamma = \iint \vec{n} \cdot (\nabla \times \vec{V}) dS$, where $\vec{n}$ is the unit vector in the direction perpendicular to the cross-sectional area *(S)* in which the vorticity ($\nabla \times \vec{V}$) is measured.

Thus, the circulation is used to measure the total vorticity flux across the cross-sectional area and to provide a quantitative evaluation of the strength (magnitude) of the rota-

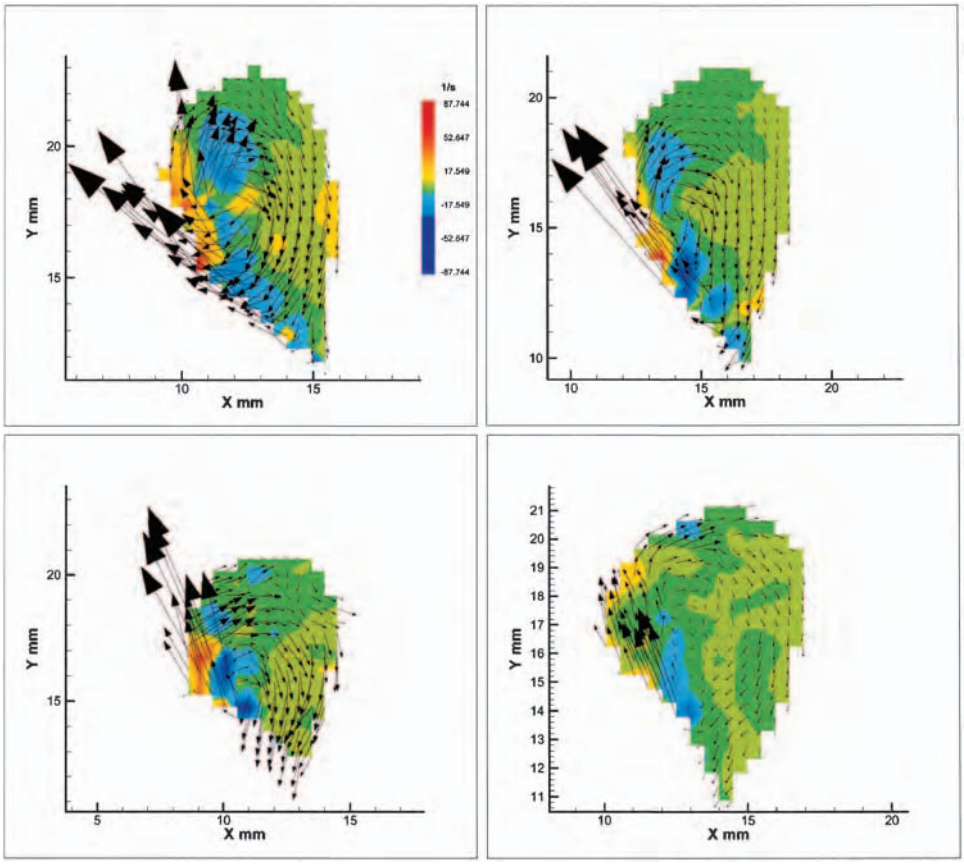

FIG. 9. Graphs showing a comparison of the shear stress fields at peak systole corresponding to the control model *(upper left)* and the experimental models after placement of one *(upper right)*, two *(lower left)*, and three *(lower right)* stents.

tional motion inside the sac. Note that, based on the velocity measurements given in Fig. 5, the strength of the clockwise vortex within the sac varies as one moves along the cardiac cycle, reaching a maximum at peak systole. Thus, the circulation Γ varies periodically with each cardiac cycle.

We measured the evolution of the circulation inside the aneurysm over time in the control model, as well as in the experimental models after placement of each stent. Figure 11 *upper* shows the circulation measured for the control model during three consecutive cardiac cycles. The negative values simply reflect the standard sign convention used in mechanics: positive vorticity for the counterclockwise rotation and negative vorticity for the clockwise rotation. Apparent from these measurements is the fact that, although the circulation reached a maximum at the peak systole, it never vanished during the diastole; thus indicating the persistence of the rotational motion inside the sac during the entire cardiac cycle. The persistence of the rotational motion inside the sac was preserved while we placed the stents. Nevertheless, one should observe that when we plotted the absolute values of the circulation for the comparison of the control model with the stented models (Fig. 11), we found that the circulation decreased dramatically when the first stent was placed and was somehow reduced when the second and third stents were implanted. Placement of one stent led to a reduction in the circulation of 68.4%, whereas placement of two or three stents led to a global reduction of, at most, 85.6%. These measurements are consistent with the results shown in Table 1.

Discussion

Stent technology was originally developed to be used in the coronary circulation[16] to prevent occlusion and restenosis after transluminal angioplasty. Due to its success in that field, tremendous progress has been made to modify the

TABLE 1

Comparison of maximal mean values of velocity, vorticity, and strain rate fields at both peak systole and peak diastole

Variable	Velocity Magnitude (m/second)	Vorticity (1/second)	Strain Rate (1/second)
peak systole			
control	0.30 ± 0.011	187.07 ± 15.29	80 ± 7.76
1st stent placed	0.22 ± 0.030	137.14 ± 29.40	58.70 ± 8.86
2nd stent placed	0.24 ± 0.018	155.95 ± 9.02	70.25 ± 15.74
3rd stent placed	0.13 ± 0.016	79.07 ± 6.49	38.39 ± 6.25
peak diastole			
control	0.08 ± 0.003	34.85 ± 1.87	12.21 ± 0.70
1st stent placed	0.02 ± 0.004	12.46 ± 3.68	5.47 ± 0.78
2nd stent placed	0.03 ± 0.005	20.78 ± 5.18	8.38 ± 1.21
3rd stent placed	0.02 ± 0.003	11.71 ± 1.76	4.72 ± 0.62

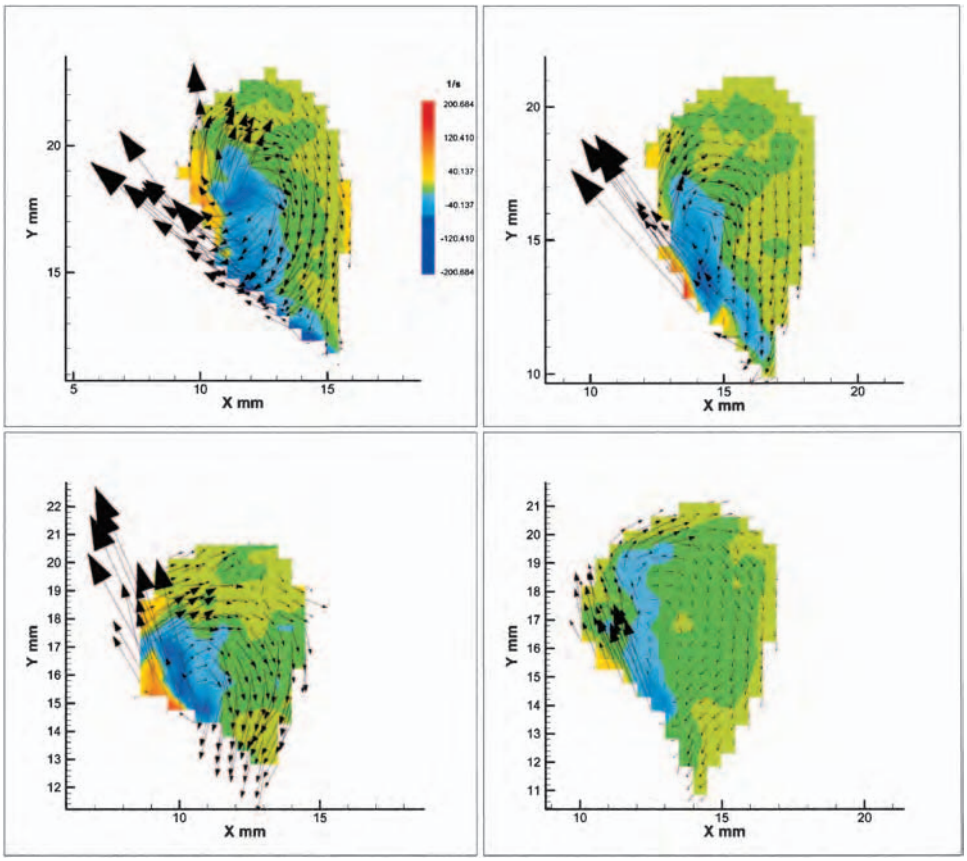

FIG. 10. Graphs demonstrating a comparison of the vorticity fields at peak systole corresponding to the control model *(upper left)* and the experimental models after placement of one *(upper right)*, two *(lower left)*, and three *(lower right)* stents.

design of stents so they can be used in the treatment of aneurysms in the intracranial circulation. Nevertheless, the extension of stent technology to the intracranial vasculature has been limited until recently by the lack of availability of stents and stent delivery systems capable of safe, effective navigation to the intracranial vessels. Recently, an improved stent design and better system delivery technology have allowed access to the tortuous vascular segments of the intracranial system. In this study, we made use of one of these novel designs; we used the flexible Neuroform stents developed by Boston Scientific/Target.

More than 200 Neuroform stents have been implanted worldwide. Although early experience with the initial generation of Neuroform was plagued with frequent implantation failures,[6,8] experience accumulated with stent-supported coil embolization and stent monotherapy since the release of Neuroform 2[2,6,15] has supported the utility of the device in treating wide-necked aneurysms. This experience has also lead to the identification of a low likelihood of significant complications related to injury to a perforating or parent vessel, aside from issues associated with the underutilization of appropriate antiplatelet therapy in cases in which placement of a stent is desired.

It has been argued that the high porosity of intravascular stents may limit aneurysm thrombosis following primary stent placement.[11] To prepare for this contingency, there are some reports on investigators' experiences in placing more than one stent,[3,5] but there is not any evidence about the optimal number of stents needed to avoid aneurysm growth or rupture.

Our study represents a systematic, quantitative evaluation of the flow changes occurring inside an aneurysm as a result of placing one, two, and even three stents. We compared the effect of increasing the number of stents placed across the neck of a sidewall aneurysm on the velocity, vorticity, and stress fields inside the aneurysm sac. We measured a consistent decrease in the values of the maximal averaged velocity, vorticity, and stress. This decrease was measured in three different sets of velocity measurements obtained in two different sidewall aneurysm models, although we only report the results from one of these models here. Measurements of the circulation inside the sac showed a systematic reduction in the strength of the vortex due to the stent placement. This decrease was especially remarkable after the first stent had been implanted. Placement of two or three stents also led to a reduction in the magnitude of the mentioned quantities, but this reduction was much less significant.

The reduction in the shear stresses and in the circulation, resulting from the implantation of the first stent could also be due to slight changes in the curvature of the parent vessel caused by the guidewire and the catheter during stent implantation, by the stent itself, or by both the implantation tools and the stent. This additional effect could be the reason for the nonlinear decrease in the circulation with place-

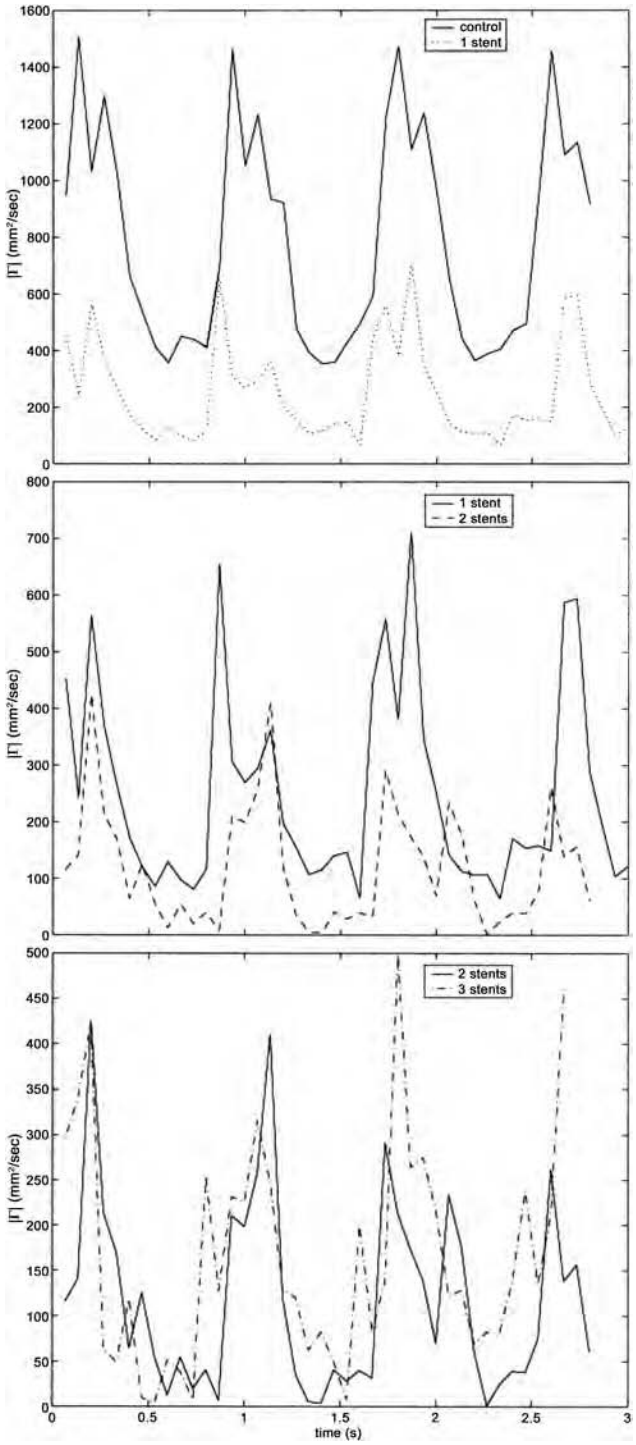

FIG. 11. Graphs demonstrating a comparison of the change with time of the absolute value of the circulation for the control model and the experimental models. *Upper:* Changes in circulation due to the placement of one stent. *Center:* Changes due to two stents. *Lower:* Changes due to three stents.

ment of each consecutive stent and for the large variability observed from measurement to measurement, which was as high as 22.4%, as indicated in Table 1.

Considering that a decrease in the porosity of the mesh may lead to an excessive neointimal response, with a risk of secondary stenosis of the artery in a high stent metal-to-arterial tissue ratio,[13,18] our results should be complemented with a clinical study that could establish the threshold for aneurysm occlusion as well as the risk of stenosis to determine the optimal number of stents needed to prevent aneurysm growth or rupture.

We have also described the flow pattern encountered in sidewall aneurysms and its changes while placing stents across the aneurysm neck. The existence of a vortex forming at the distal neck and moving toward the dome has already been reported elsewhere[1,12–14,17] and has been confirmed in this study.

Conclusions

In this paper we report the effect of placing multiple stents on the hemodynamics of a sidewall aneurysm model by measuring the velocity field inside the aneurysm sac of the model. Our measurements demonstrate that the use of multiple flexible intravascular stents effectively reduces the strength of the vortex forming in the aneurysm sac with a subsequent decrease in the magnitude of the stresses acting on the aneurysm wall. Therefore, placement of multiple stents may induce thrombosis as well as decrease the risks of aneurysm growth and/or rupture.

Disclosure

David Levy, M.D., is a consultant for Boston Scientific Corp. and receives financial compensation. In addition, Prof. Lasheras' laboratory has received a donation from Boston Scientific Corp. to perform these experiments.

References

1. Aenis M, Stancampiano AP, Wakhloo AK, Lieber BB: Modeling of flow in a straight stented and nonstented side wall aneurysm model. **J Biomech Eng 119:**206–212, 1997
2. Benitez RP, Silva M, Klem J, Veznedaroglu E, Rosenwasser RH: Endovascular occlusion of wide-necked aneurysms with a new intracranial microstent (Neuroform) and detachable coils. **Neurosurgery 54:**1359–1368, 2004
3. Benndorf G, Herbon U, Sollmann WP, Campi A: Treatment of a ruptured dissecting vertebral artery aneurysm with double stent placement: case report. **AJNR Am J Neuroradiol 22:** 1844–1848, 2001
4. Cantón G, Levy DI, Lasheras JC: Hemodynamic changes due to stent placement in bifurcating intracranial aneurysms. **J Neurosurg 103:**146–155, 2005
5. Doerfler A, Wanke I, Egelhof T, Stolke D, Forsting M: Double-stent method: therapeutic alternative for small wide-necked aneurysms. Technical note. **J Neurosurg 100:**150–154, 2004
6. Fiorella D, Albuquerque FC, Han P, McDougall CG: Preliminary experience using the Neuroform stent for the treatment of cerebral aneurysms. **Neurosurgery 54:**6–17, 2004
7. Geremia G, Haklin M, Brennecke L: Embolization of experimentally created aneurysms with intravascular stent devices. **AJNR Am J Neuroradiol 15:**1223–1231, 1994
8. Howington JU, Hanel RA, Harrigan MR, Levy EI, Guterman LR, Hopkins LN: The Neuroform stent, the first microcatheter-delivered stent for use in the intracranial circulation. **Neurosurgery 54:** 2–5, 2004
9. Kerber CW, Heilman CB, Zanetti PH: Transparent elastic arterial models I: A brief technical note. **Biorheology 26:**1041–1049, 1989
10. Lanzino G, Wakhloo AK, Fessler RD, Hartney ML, Guterman

LR, Hopkins LN: Efficacy and current limitations of intravascular stents for intracranial internal carotid, vertebral, and basilar artery aneurysms. **J Neurosurg 91:**538–546, 1999
11. Lanzino G, Wakhloo AK, Fessler RD, Mericle RA, Guterman LR, Hopkins LN: Intravascular stents for intracranial internal carotid and vertebral artery aneurysms: preliminary clinical experience. **Neurosurgical Focus 5(4):**E3, 1998
12. Lieber BB, Livescu V, Hopkins LN, Wakhloo AK: Particle image velocimetry assessment of stent design influence on intra-aneurysmal flow. **Ann Biomed Eng 30:**768–777, 2002
13. Lieber BB, Stancampiano AP, Wakhloo AK: Alteration of hemodynamics in aneurysm models by stenting: influence of stent porosity. **Ann Biomed Eng 25:**460–469, 1997
14. Liou TM, Chang WC, Liao CC: LDV measurements in lateral model aneurysms of various sizes. **Exp Fluids 23:**317–324, 1997
15. Lylyk P, Ferrario A, Pasbón B, Miranda C, Doroszuk G: Buenos Aires experience with the Neuroform self-expanding stent for the treatment of intracranial aneurysms. **J Neurosurg 102:**235–241, 2005
16. Sigwart U, Puel J, Mirkovitch V, Joffre F, Kappenberger L: Intravascular stents to prevent occlusion and restenosis after transluminal angioplasty. **N Engl J Med 316:**701–706, 1987
17. Tateshima S, Viñuela F, Villablanca JP, Murayama Y, Morino T, Nomura K, et al: Three-dimensional blood flow analysis in a wide-necked internal carotid–ophthalmic artery aneurysm. **J Neurosurg 99:**526–533, 2003
18. Tominaga R, Harasaki H, Sutton C, Emoto H, Kambic H, Hollman J: Effects of stent design and serum cholesterol level on the restenosis rate in atherosclerotic rabbits. **Am Heart J 126:** 1049–1058, 1993
19. Wakhloo AK, Lanzino G, Lieber BB, Hopkins LN: Stents for intracranial aneurysms: the beginning of a new endovascular era? **Neurosurgery 43:**377–379, 1998
20. Yu SCM, Zhao JB: A steady flow analysis on the stented and nonstented sidewall aneurysm models. **Med Eng Phys 21:**133–141, 1999

Manuscript received September 2, 2004.
Accepted in final form June 7, 2005.

Address reprint requests to: Gádor Cantón, Ph.D., Department of Mechanical and Aerospace Engineering, University of California, San Diego, 9500 Gilman Drive, MC 0411, La Jolla, California 92093-0411. email: gcanton@mae.ucsd.edu.